Techniques to accelerate thermo-mechanical simulations in large-scale FE models with nonlinear plasticity and cyclic input

IOP Conf. Series: Materials Science and Engineering **629** (2019) 012008 doi:10.1088/1757-899X/629/1/012008

Techniques to accelerate thermo-mechanical simulations in large-scale FE models with nonlinear plasticity and cyclic input

D Benasciutti[1,3], F De Bona[2], L Moro[2] and J Srnec Novak[2]

[1]Department of Engineering, University of Ferrara, via Saragat 1, 44122 Ferrara, Italy
[2]Politechnic Department of Engineering and Architecture (DPIA), University of Udine, via delle Scienze 208, 33100 Udine, Italy

E-mail: denis.benasciutti@unife.it

Abstract. A procedure is proposed to reduce the computation time of thermo-mechanical simulations with large nonlinear finite element (FE) models that involve cyclic plasticity. The procedure is helpful when it is practically unfeasible to simulate the huge amount of cycles needed to bring the material model to its fully stabilised state (an unfavourable situation that often occurs when small plastic strains are present), as required before assessing the structural durability. A "reference" test case, with combined kinematic and isotropic nonlinear model calibrated on actual material properties, is compared to accelerated models as well as pure kinematic models. Guidelines on how to set up the accelerated model are finally discussed.

1. Introduction

Structural durability of complex structures undergoing cyclic thermo-mechanical loadings may exploit results from elasto-plastic finite element (FE) analyses. On the one hand, the fatigue life assessment requires that the simulated cyclic material behavior reaches its complete stabilized condition (which occurs about at half the number of cycles to failure). On the other hand, attaining such a stabilized condition in large-scale nonlinear FE models may require that a huge number of cycles are simulated, which may become computationally unfeasible.

In a recent study dealing with elasto-plastic analysis of a copper mold for steelmaking plant [1], it was estimated that the three-dimensional FE model would had required thousands of cycles (around 60000) to simulate the material behavior until complete stabilization, due to the unfavorable combination of small plastic strains and low stabilization speed of the mold alloy. In turn, thousands of cycles would have last hundreds of simulation days, i.e. beyond any practical limit.

The use of accelerated material models, as proposed in [2], was considered a mean to keep the computation time within more acceptable limits. In accelerated models, the stabilization speed is increased up to a "fictitious" value (see figure 1), which permits the number of cycles for simulating the material behavior from the onset of plasticization up to the stabilized condition to be reduced considerably (and so the computation time, too). In some cases, however, the stabilization speed cannot be increased arbitrarily and unreasonably (figure 1) if one needs to prevent numerical converge issues or "unrealistic" results in simulations [2].

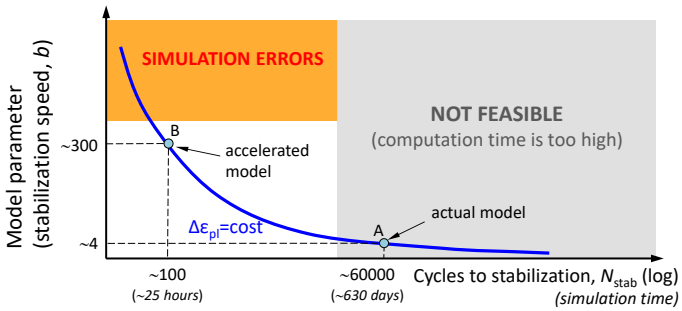

Figure 1. Actual and accelerated model. Simulation time is decreased if the stabilization speed b is increased from its actual value (A) to a "fictitious" value (B).

Checking the correctness of acceleration techniques is possible only by comparison with a "reference" case that permits the cyclic material behavior to be simulated until complete stabilization. In this work, the reference case is an axisymmetric FE model of a hollow copper mold subjected to cyclic thermal loadings.

2. Plasticity model: Theoretical background

The cyclic material behaviour is modelled through a combined kinematic and isotropic model [3]:

$$\sqrt{\frac{3}{2}(\boldsymbol{S}-\boldsymbol{X}):(\boldsymbol{S}-\boldsymbol{X})}-R-\sigma_0=0 \tag{1}$$

where $\boldsymbol{S}$ is the deviatoric stress tensor, $\boldsymbol{X}$ is the deviatoric back-stress tensor, R is the drag stress and σ_0 is the initial yield stress. In the combined model, the yield surface both translates (controlled by $\boldsymbol{X}$) and expands (controlled by R) as function of plastic strain increment $\mathrm{d}\boldsymbol{\varepsilon}_{\mathrm{pl}}$ and accumulated plastic strain $\varepsilon_{\mathrm{pl,acc}}$. The kinematic part is based on the Chaboche's nonlinear model [3]:

$$\boldsymbol{X}=\sum_{\mathrm{i}=1}^{n}\boldsymbol{X}_{\mathrm{i}} \qquad ; \qquad \mathrm{d}\boldsymbol{X}_{\mathrm{i}}=\frac{2}{3}C_{\mathrm{i}}\mathrm{d}\boldsymbol{\varepsilon}_{\mathrm{pl}}-\gamma_{\mathrm{i}}\boldsymbol{X}_{\mathrm{i}}\mathrm{d}\varepsilon_{\mathrm{pl,acc}} \tag{2}$$

where C is the hardening modulus and γ is the recovery parameter controlling the decay of C as plastic strain accumulates. For i=1, equation (2) yields the Armstrong-Frederick model with only two pairs (C_1, γ_1). For γ=0, equation (2) gives the Prager model (linear kinematic), in which $\mathrm{d}\boldsymbol{X}=(2/3)C_{\mathrm{lin}}\mathrm{d}\boldsymbol{\varepsilon}_{\mathrm{pl}}$.

The isotropic model, which controls the material hardening/softening, is based on the incremental relationship $\mathrm{d}R=b(R_\infty-R)\mathrm{d}\varepsilon_{\mathrm{pl,acc}}$, in which R_∞ is the saturated stress and b is the stabilization speed for hardening ($R_\infty>0$) or softening ($R_\infty<0$). Integrating the previous expression gives [3]:

$$R=R_\infty\left[1-\exp\left(-b\varepsilon_{\mathrm{pl,acc}}\right)\right] \tag{3}$$

The material stabilizes when R reaches R_∞, which (according to [3]) occurs approximately when the exponent $b\varepsilon_{\mathrm{pl,acc}}\cong 5$. In strain-controlled fully reversed cycles characterized by a plastic strain range $\Delta\varepsilon_{\mathrm{pl}}$, the total plastic strain accumulated after N cycles is approximately $2N\Delta\varepsilon_{\mathrm{pl}}$ and the stabilized condition becomes $2bN_{\mathrm{stab}}\Delta\varepsilon_{\mathrm{pl}}\cong 5$ (where N_{stab} is the number of cycles to stabilization). This relationships shows that N_{stab} is inversely proportional to both b and $\Delta\varepsilon_{\mathrm{pl}}$ (see figure 1) and explains why N_{stab} may become really large in those situations in which plastic strain accumulates rather slowly, due to a material that has a small b and is subjected to cycles where plastic strain is not predominant.

Increasing b is but one of many techniques proposed in literature. If both creep and thermal fatigue are present, some authors [4,5] suggest that only a limited number of cycles can be simulated. Although not well defined, this procedure could be justified by considering that visco-elasticity tends to reduce the time to stabilization. If creep rupture constitutes the damage criterion in design, an extrapolation

technique aimed to speed up the simulation is proposed in [6]. In situations with no creep, other authors [7,8] adopt a kinematic model with stabilized material properties from the beginning of simulation (no isotropic model simulates the cyclic material hardening/softening).

3. Numerical case study

3.1. Component description

As benchmark, numerical simulations consider a mold for continuous casting of steel, which is a hollow tube where the initial solidification of steel takes place (see figure 2(a)). The actual shape of mold cross section (round, square, rectangular) depends on the shape of the final product. On its inner surface, the component is subjected to a massive thermal flux q that varies along its length, from a maximum q_{max} (corresponding to the position of liquid steel) to a constant value. The overall thermal flux distribution also changes over time, from its full value (plant is in service) to zero (plant switched off). On its outer surface, the mold is water-cooled. The component is simply supported to the surrounding structure and is free to expand. Molds are made of copper alloys, as they have a favorable combination of high thermal conductivity and good mechanical strength. The mold analyzed in this study has length 1000 mm, inner diameter 200 mm and thickness 16 mm, and it is made of CuAg0.1 alloy, whose cyclic plasticity properties (estimated from experiments) are summarized in [9].

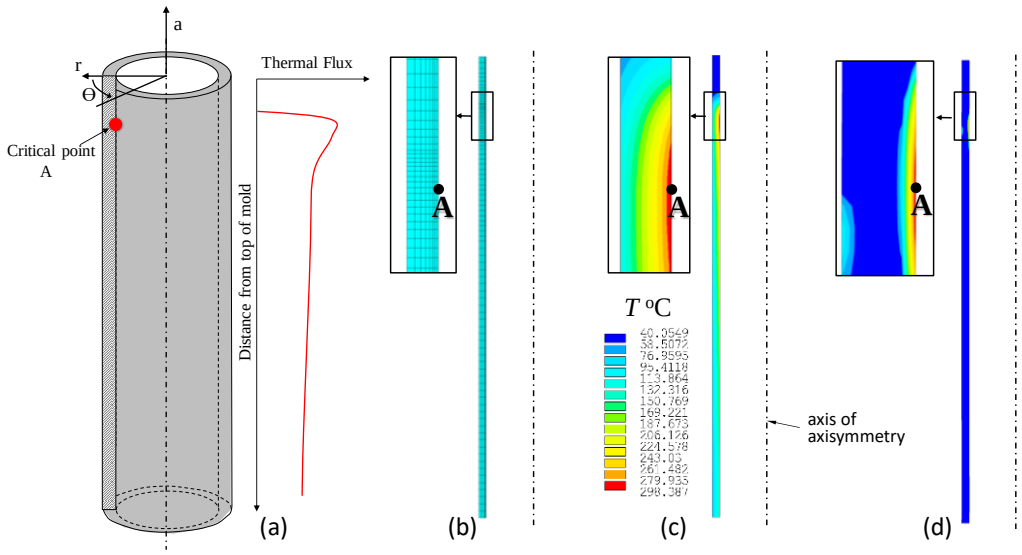

Figure 2. (a) component; (b) axisymmetric finite element model and mesh zoom; (c) temperature distribution; (d) equivalent plastic strain distribution.

3.2. Finite element model

Thanks to the axial symmetry of geometry and boundary conditions, the mold can be represented by a two-dimensional (2D) axisymmetric FE model (see figure 2(b)), which moreover permits the computation time to be greatly reduced even when simulating hundreds of cycles. The model is constituted by 760 axisymmetric 8-node isoparametric elements, for a total of 2487 nodes. Mesh is refined in the region of maximum thermal flux (point A), where the highest temperatures and stress gradients are expected to occur. The mold thermo-mechanical response is simulated by a first thermal analysis that yields the temperature distribution, which is then input in following mechanical analysis.

3.3. Thermal analysis results

In thermal analysis, a thermal flux of 3.2 MW/m^2 proposed in [10] is applied on the inner surface, a convection on the outer surface (with bulk temperature 40°C and convection coefficient 48000 W/m^{2}K).

The thermal flux from [10] was incremented by about 50% so that the maximum temperature reached the value 300°C for which material properties are available in [9]. The model also includes temperature dependent material properties. The change of heat flux is simulated by a sequence of steady-state analyses, are explained in [1].

Figure 2(c) displays the calculated temperature distribution. The largest temperature gradients are located close to the region of maximum thermal flux, where also the maximum temperature 298°C occurs at point A (this point will be monitored in structural analysis).

3.4. Mechanical analysis results

The input is the temperature field calculated in previous thermal analysis. No mechanical constraints are applied to the model, as the actual mold is free to expand. A nonlinear combined kinematic and isotropic material model is used and brought up to complete stabilization ("reference" case). Material parameter values are taken from [9] (the CuAg01 exhibits cyclic softening).

Results from the "reference" case were compared to those from other models, namely:

- accelerated (combined kinematic-isotropic) models, with an increased stabilization speed b_a. In order to make the sensitivity analysis the widest possible, eight values – covering a wider range than that suggested in [2] – were scrutinized (b_a=0.01b, 10b, 20b, 30b, 100b, 200b, 300b, 421b);
- only kinematic model (linear) according to Prager;
- only kinematic model (nonlinear), with the static parameters calibrated on either first or stabilized cycle;

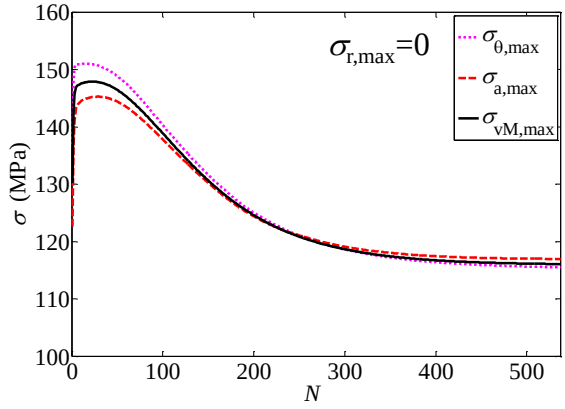

Figure 3. Stress components vs. loading cycles.

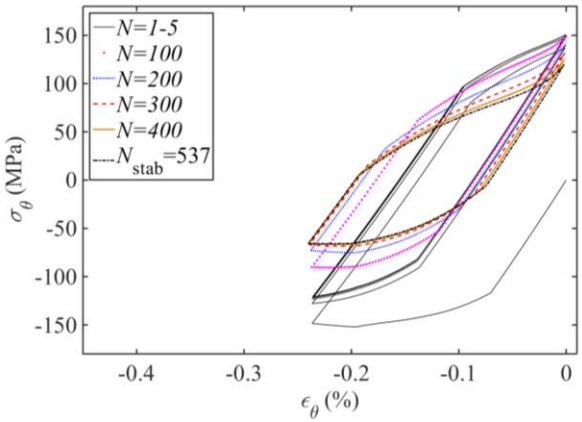

Figure 4. Evolution of hoop stress-strain at cycles (for clarity, only some cycles are plotted).

For accelerated model, the value 0.01b represents a lower bound for which the contribution of isotropic part to the combined model becomes negligible (i.e. material does not show softening). By contrast, value 421b constitutes an upper bound for which cyclic softening occurs so rapidly that – as it will be discussed later on – unrealistic results ("distorted" stress-strain cycles) are obtained (for even higher b, simulation do not converge at all). For Prager and nonlinear kinematic models, the difference in material properties between initial state and stabilized state are considered by calibrating the elastic modulus and yield stress either on the first cycle (E_1, σ_0) or on the stabilized cycle (E_s, σ_{0*}). Note that the first quarter of first cycle corresponds to the monotonic uniaxial stress-strain curve.

The "reference" combined model takes about 537 cycles to make the material stabilize (adopting the stabilization criterion described in [11]), as also confirmed by the cyclic evolution of stress components (radial, hoop and axial stress), see figure 3. Figure 4 depicts the evolution of hoop stress-hoop strain cycles at certain intervals (for more clarity, not all cycles are shown). The change of shape thorough cycling is evident.

Figure 5 shows how, for various accelerated models, the maximum von Mises stress in each cycle

changes over the applied cycles N (which are normalized to the cycles N_{stab} required to complete stabilization, in order to better emphasize the various trends in the very first cycles). All models attain almost the same asymptotic stress value, except the model with b_a=0.01b in which the isotropic model, is somehow "deactivated". It follows that the material to exhibit any softening (the hardening shown is only due to the kinematic model and ends in the first 8 cycles).

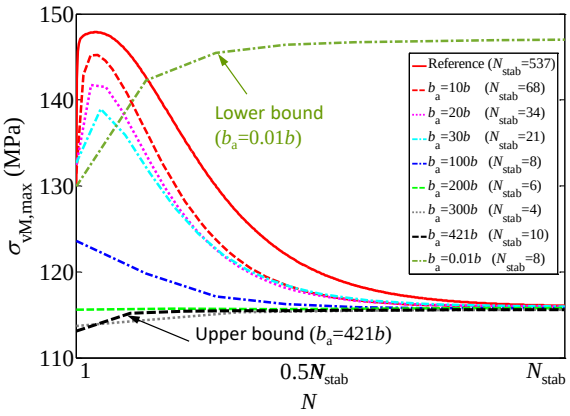

Figure 5. Evolution of max. von Mises stress over cycles for different accelerated models.

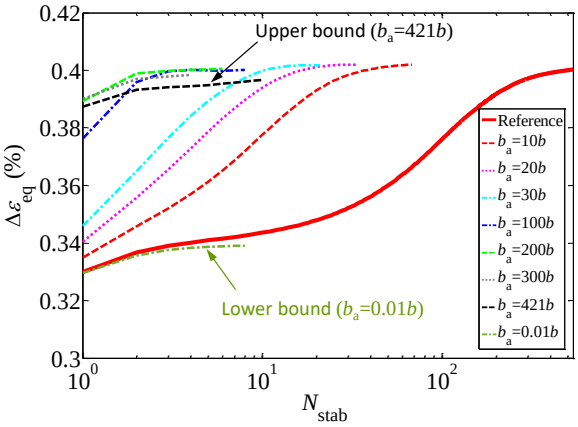

Figure 6. Evolution of equivalent strain range over cycles for different accelerated models.

Of more interest is to monitor the evolution of the equivalent strain range $\Delta\varepsilon_{eq}$ as defined in [12] (see figure 6), as this parameter is used to assess the low-cycle fatigue life. For the "reference" model (not accelerated), the strain range $\Delta\varepsilon_{eq}$ increases throughout the whole loading cycles, with a maximum rise of about 18%. This trend confirms that, if cyclic loading is stopped before material had reached complete stabilization and $\Delta\varepsilon_{eq}$ attained its asymptotic value, the fatigue life may be overestimated (in a Manson-Coffin curve, the life is indeed a nonlinear inverse function of strain range as $\Delta\varepsilon_{eq}^{-c}$, where c is a material parameter). Models with a stabilization speed only moderately increased (b_a=10b÷30b) display a trend similar to the "reference" case, whereas others with much higher values (b_a=100b÷300b) follow a different behavior, in which stabilization is almost completed in the early cycles. In all models examined, though, the equivalent strain range never stays constant during cycles, which confirms how important is that, in simulations, the material reaches its stabilized state in order to avoid errors in following fatigue life assessment.

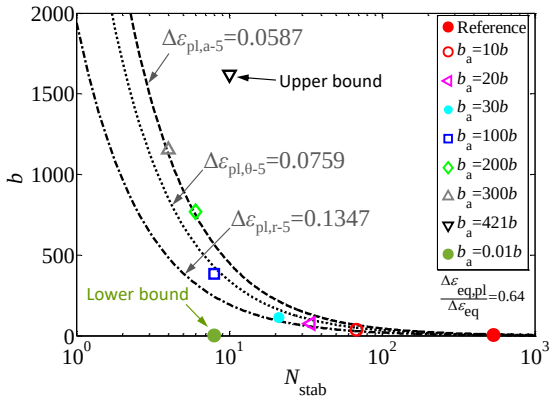

Figure 7. Design diagram for T=300°C.

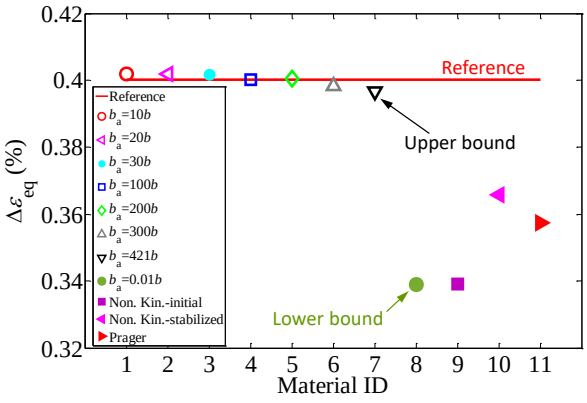

Figure 8. Comparison of $\Delta\varepsilon_{eq}$ from all models.

Figure 7 represents a sort of "design diagram" that applies the concepts sketched in figure 1. It correlates parameters b, N and $\Delta\varepsilon_{pl}$ through the relationship $2bN_{stab}\Delta\varepsilon_{pl}\cong 5$. The plastic strain range is calculated at the 5th simulated cycle. The three curves correspond to the three plastic strain range components ($\Delta\varepsilon_{pl,a}$=0.0554% axial, $\Delta\varepsilon_{pl,\theta}$=0.0734% hoop, $\Delta\varepsilon_{pl,r}$=0.1289% radial). Except for the two bound cases (b_a=0.01 and b_a=421b), the other points lie close to the analytical curves, whose validity is thus confirmed.

Table 1. Number of cycles to stabilization and $\Delta\varepsilon_{eq}$ for point A (T=300°C).

Material ID		1	2	3	4	5	6	7	8	9	10	11
	Comb. model	Accelerated models								NKI[a]	NKS[b]	Prager model
		10b	20b	30b	100b	200b	300b	421b	0.01b			
N_{stab}	537	68	34	21	8	6	4	10	8	8	10	5
$\Delta\varepsilon_{eq}$ (%)	0.400	0.402	0.402	0.402	0.400	0.401	0.398	0.397	0.339	0.339	0.366	0.357
Δe (%)		0.41	0.40	0.36	-0.02	0.5	-0.48	-0.91	-15.30	-15.26	-8.60	-10.71

[a] NKI – nonlinear kinematic model with initial parameters
[b] NKS - nonlinear kinematic model with stabilized parameters

Figure 8 compares the equivalent strain range $\Delta\varepsilon_{eq}$ in the stabilized state, from all the material models examined (pure kinematic models–both linear and nonlinear–are included, too). The values of $\Delta\varepsilon_{eq}$ provide an indirect measure of structure durability, as they are inversely proportional to the low-cycle fatigue life in a Manson-Coffin diagram. Values from figure 8 are also listed in Table 1.

Accelerated models yield comparable $\Delta\varepsilon_{eq}$ (with a maximum relative deviation of 0.5% from the "reference" case), which in turn confirms that a moderate increase of the stabilization speed (below the upper bound b_a=421b) would leave the estimated fatigue life unaltered if compared to the life estimated by the "reference" model. The upper bound value, of course, cannot be determined beforehand and needs be established for the specific engineering application under study.

Of more interest is to observe how pure kinematic models always underestimate the $\Delta\varepsilon_{eq}$ of the "reference" case, with a maximum deviation up to 15%. The lowest $\Delta\varepsilon_{eq}$ comes from the nonlinear kinematic model considering "initial" state of material (E_1, σ_0). Only a small improvement yet occurs if the nonlinear kinematic model is calibrated based on static parameters obtained from the stabilized state, or it is replaced by the linear Prager model calibrated on the initial state.

Either way, it seems apparent that neglecting the isotropic part in the combined model does not seem very appropriate. One the one hand, using a linear kinematic model greatly simplifies the model calibration, as only the monotonic tensile curve is required without any cyclic experimental data. On the other hand, figure 8 confirms the conclusions in [2], which caution engineers about the use of pure kinematic models that – regardless of being calibrated on the initial or stabilized material state – do completely neglect the material hardening/softening and the corresponding change in elastic-plastic properties over cyclic loading.

4. Guidelines for practical applications

A test case is now briefly discussed to show how accelerated models can be applied in practice. For the FE model in figure 2, the thermal flux from [10] is incremented by only 30%, so that the maximum temperature is close to the value 250°C for which material parameters (and, in particular, the stabilization speed b) are available in [9].

The relationship $2bN_{stab}\Delta\varepsilon_{pl}\cong 5$ governs the set-up of the accelerated model. To be calibrated, that relationship needs the value of plastic strain range $\Delta\varepsilon_{pl}$ in one structure point. This value can be approximated by $\Delta\varepsilon_{pl\text{-}5}$ after five cycles, which normally demands for a relatively short simulation time even with large-scale nonlinear FE models. The b parameter is known from experimental data.

The actual b value normally determines a rather high number of stabilization cycles N_{stab} (and so is

the corresponding simulation time). Therefore, after establishing a target value $N^*<N_{stab}$ that yields a more affordable simulation time, the "fictitious" $b_a \cong 5/(2N^*\Delta\varepsilon_{pl\text{-}5})$ for the accelerated model can be derived accordingly (for the example under study, $N^*=40$ gives $b_a=200$), see figure 9. Running 40 cycles with b_a gives an equivalent strain range $\Delta\varepsilon_{eq}=0.3144\%$, which only deviates by 2.27% from the value obtained by simulating 1033 cycles with the actual b. This result then validates the procedure.

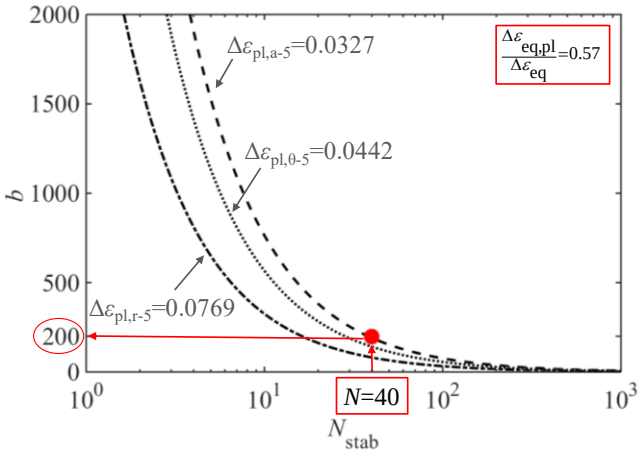

Figure 9. Design diagram for T=250°C [11].

5. Conclusions

Selecting the most appropriate cyclic plasticity model is a crucial step in thermo-mechanical finite element analysis. It may happen that the material model that fits more closely the experimental cyclic plasticity behavior is also the one that, in finite element simulations, requires a too large number of cycles to reach its stabilized state. This would result in a very long computation time, especially with large-scale three-dimensional FE models.

This work implemented several plasticity models (combined kinematic and isotropic, accelerated, Prager and nonlinear kinematic with "initial" and "stabilized" parameters) and compared them in terms of the equivalent strain range. As a basis for comparison, a "reference" test case was considered, in which the plasticity model is fitted on actual experimental data and the simulation carried out until complete material stabilization. The comparison showed that pure kinematic models, even if calibrated on either the initial or stabilized material state, deviated from the "reference" equivalent strain range, thus overestimating the actual structure fatigue life. Pure kinematic models, neglecting the material hardening/softening, seem inadequate and their use not recommended. By contrast, accelerated kinematic-isotropic models were always closed to the "reference" case, if the stabilization speed is increased up to two orders of magnitude (which allows the computation time to be shortened significantly). Guidelines were finally provided on how, in practical numerical cases, the "increased" stabilization speed in accelerated models can properly be set up.

References

[1] Srnec Novak J, Benasciutti D, De Bona F, Stanojević A and Huter P 2015 *Procedia Engineering* **133** 688-97
[2] Chaboche J L and Cailletaud G 1986 *Comput. Struct.* **23** 23-31
[3] Chaboche J L 2008 *Int. J. Plasticity* **24** 1642-93
[4] Arya V K, Melis M E and Halford G R 1990 *Finite Element Elastic-Plastic-Creep and Cyclic Life Analysis of a Cowl Lip* (NASA Technical Memorandum 102342)
[5] Amiable S, Chapuliot S, Constantinescu A and Fissolo A 2006 *Fatigue Fract. Eng. Mater. Struct.* **29** 209-17
[6] Kontermann C, Scholz A and Oechsner M 2014 *Mater. High Temp.* **31** 334-42

[7] Li B, Reis L and de Freitas M 2006 *Int. J. Fatigue* **28** 451-8
[8] Campagnolo A, Berto F and Marangon C 2016 *Theor. Appl. Fract. Mec.* **81** 76-88
[9] Benasciutti D, Srnec Novak J, Moro L, De Bona F and Stanojević A 2018 *Fatigue Fract. Eng. Mater. Struct.* **41** 1364-77
[10] Galdiz P, Palacios J and Thomas B G 2014 *Proc. European Cont. Casting Conf.* (Graz, Austria, June 23–26, 2014)
[11] Srnec Novak J, De Bona F, Benasciutti D and Moro L 2018 *MATEC Web of Conf.* **165** 19010
[12] Manson S S 1966 *Thermal Stress and Low-cycle Fatigue* (New York: McGraw-Hill)